Axisymmetric Static and Dynamic Buckling of Spherical Caps due to Centrally Distributed Pressures

WENDELL B. STEPHENS* AND ROBERT E. FULTON†
NASA Langley Research Center, Hampton, Va.

Sanders' axisymmetric nonlinear elastic shell theory, including provision for general orthotropy along the shell meridian, is approximated by finite difference equations including the Houbolt backward difference formulation in time. The equations are then applied to the nonlinear response of an isotropic shallow spherical cap subjected to static and dynamic loads. Axisymmetric static buckling is determined by investigating the convergence characteristics of the static numerical solution as the "top of the knee" buckling point is reached. Dynamic buckling is defined as the threshold load at which large increases in the peak amplitude of the average dynamic displacement occur. Axisymmetric buckling loads are given for a spherical cap subjected to a constant static pressure or step pulse of infinite duration distributed axisymmetrically over a portion of the center of the shell. The influence of the size of the loaded area and of moment and inplane boundary conditions on both static and dynamic buckling is studied, as well as the use of various criteria to define the threshold load for dynamic buckling.

Nomenclature

A_L = surface area of the shell subjected to a load
A_S = surface area of the shell
C_{ij},D_{ij},K_{ij} = orthotropic material constants defined in Eqs. (A7) and (A8)
E = reference modulus of elasticity
e_{11},e_{22}, $\epsilon_{11},\epsilon_{22}$ = nondimensional and dimensional membrane strains, e.g., $e_{11} = \epsilon_{11}\eta$
H_0 = maximum shell rise
h = reference thickness
m_{11},m_{22}, M_{11},M_{22} = nondimensional and dimensional bending moment in the principal directions, e.g., $m_{11} = RM_{11}/(\sigma h^3)$
n_{11},n_{22}, N_{11},N_{22} = nondimensional and dimensional membrane stress resultants, e.g., $n_{11} = N_{11}/(\sigma h)$
P = load parameter defined in Eq. (18)
P_{cr} = value of load parameter P associated with axisymmetric buckling
p_0,p_s, P_0,P_s = nondimensional and dimensional lateral and meridional forces per unit area, e.g., $p_0 = P_0R/(\sigma h)$
q,Q = nondimensional and dimensional transverse shear, $q = Q/(\sigma h)$
R = spherical shell radius
r = nondimensional radial distance from axis of symmetry to shell middle surface
r_0 = nondimensional radial distance from axis of symmetry to shell edge
$S_{\max}$ = total arc length of the shell meridian
S_L = length of loaded meridian
s,S = nondimensional and dimensional meridian distance, $s = S/R$
$t_1{}^m,t_2{}^m$ = nondimensional thermal moment resultant in the principal direction
$t_1{}^n,t_2{}^n$ = nondimensional thermal force resultant in the principal directions
u,w, U,W = nondimensional and dimensional meridional and normal displacement, respectively, e.g., $w = \eta W/R$
α_m,β_m, γ_m,δ_m = coefficients of the acceleration difference expression
$\bar{\alpha}$ = coefficient of thermal expansion
$\beta,\bar{\beta}$ = nondimensional and dimensional rotation, $\beta = \eta\bar{\beta}$
Δ = average displacement defined in Eq. (17)
$\Delta_{\max}$ = peak average displacement of the shell
$\Delta s,\Delta\tau$ = nondimensional spatial and time increments
ζ = shell thickness coordinate normal to and originating from the middle surface, positive outward
η = ratio of reference elasticity modulus to reference stress, E/σ
θ = circumferential coordinate
κ_{11},κ_{22}, k_{11},k_{22} = nondimensional and dimensional curvatures, e.g., $\kappa_{11} = R\eta k_{11}$
λ = shell parameter, $\lambda = 2\{3(1-\nu^2)\}^{1/4}\{H_0/h\}^{1/2}$
ν = Poisson's ratio for isotropic material
ξ = undeformed shell rise at any point r
ρ = ratio of reference thickness to reference length, h/R
ρ_0 = mass density
σ = reference stress
τ,t = nondimensional and dimensional time, $\tau = (E/\rho_0R^2)^{1/2}t$
τ^* = length of time load is applied from $\tau = 0$
φ = colatitude coordinate of a point on the shell meridian
φ_L = colatitude coordinate describing load distribution (Fig. 1)
φ_0 = colatitude coordinate of shell boundary
$H,\tilde{H},f$ = 6×6 matrices
Ω,Λ = 3×3 matrices
$z,\dot{z},\ddot{z}$, $\bar{z},\delta z,e$ = 6×1 column matrices
$x,y,\bar{x},y$, $\delta x,\delta y,l$ = 3×1 column matrices

Presented as Paper 69-89 at the AIAA 7th Aerospace Sciences Meeting, New York, January 20–22, 1969; submitted February 6, 1969; revision received April 15, 1969.

* Aerospace Engineer. Member AIAA.
† Section Head. Member AIAA.

Introduction

AXISYMMETRIC and asymmetric buckling of spherical caps have been studied extensively in the literature for certain simplified loadings and boundary conditions. For example, results for axisymmetric buckling due to uniformly distributed static loads, dynamic impulses, or dynamic step pulses are reported in Refs. 1–8. Results for asymmetric buckling due to static uniform pressures are given in Refs. 1, 2, and 6. Results for axisymmetric buckling due to static point loads are given in Refs. 9–12 and for asymmetric buckling in Ref. 9. A comprehensive survey of the state-of-the-art for spherical cap buckling is given in Ref. 6. All these results are restricted to either concentrated loads at the apex or to uniformly distributed loads; they are also limited to classical boundary conditions. Unfortunately, the character of the buckling response for these extreme cases differs widely; the uniformly loaded shell fails violently and is sensitive to imperfections, whereas the shell under a point load deforms

gradually with load and is little affected by imperfections. Moreover, partial loading of a spherical shell occurs in practical aerospace applications as, for example, in landing impact of spacecraft. Therefore, there is a need for buckling results for static and dynamic loads that span the range between concentrated loads and uniformly distributed loads. There is also a need for further data on the influence of boundary conditions on static and dynamic buckling loads. It is well known that a complete static investigation of such effects requires the consideration of asymmetric buckling to obtain the lowest possible buckling load. This is also true for dynamic buckling as is shown for arches, for example, in Ref. 13. However, axisymmetric buckling is critical in some ranges of the shell parameters and an understanding of symmetric buckling is an important first step even where asymmetric behavior is critical. The present paper, therefore, reports on an investigation of the static and dynamic axisymmetric buckling of shallow spherical caps subjected to centrally distributed axisymmetric pressures.

Analysis

The shell analysis used in this study is based on Sanders' (Ref. 14) equations for axisymmetric behavior of an elastic shell of revolution which include geometric nonlinearities. These equations, coupled with constitutive equations that account for general orthotropy and thermal effects along the meridian, can be expressed in terms of six partial differential equations of first order in space and second order in time. These equations are of the following form:

$$Iz' + (H + \tilde{H})z = e + f\dot{z} \tag{1}$$

where z is the solution vector of six variables, I is the 6×6 identity matrix, H and $\tilde{H}$ are the linear and nonlinear 6×6 coefficient matrices of z, respectively, f is the 6×6 mass matrix of z and e is the six-element load vector. Primes indicate differentiation with respect to meridional distance, s and the dots differentiation with respect to time, τ. The elements of H, $\tilde{H}$, e, f, and z are listed in the Appendix in the nondimensional format of Ref. 15. (Relations between the nondimensional and dimensional expressions are also given in the Nomenclature.)

The general set of shell boundary conditions for Eq. (1) at an edge can be written as

$$\Omega x + \Lambda y - l = 0 \tag{2}$$

where x and y are force and displacement subvectors of z defined in the Appendix, Ω and Λ are 3×3 matrices, and l is a three-element vector.

Equation (1) is converted into difference equations utilizing central differences for the spatial derivatives and Houbolt's backward differences (Ref. 16) for the time derivatives. The spatial finite difference representations are written at a point halfway between stations and are of the form

$$z_{i-\frac{1}{2}} = (z_i + z_{i-1})/2 \tag{3}$$

$$z'_{i-\frac{1}{2}} = (z_i - z_{i-1})/\Delta s \tag{4}$$

The second-order time derivative in Eq. (1) is approximated by

$$\ddot{z}_{i,m} = (\alpha_m z_{i,m} + \beta_m z_{i,m-1} + \gamma_m z_{i,m-2} + \delta_m z_{i,m-3})/\Delta\tau^2 \tag{5}$$

In Eqs. (3–5) the subscripts i and m indicate spatial and time stations, respectively, and Δs and $\Delta\tau$ are the spatial and time increments, respectively. The coefficients α_m, β_m, γ_m, and δ_m depend on the time step and are given in Ref. 17. Application of the finite difference approximations (3–5) to Eq. (1) leads to a set of six nonlinear algebraic equations for z at the mth time step:

$$f_k(z_{i,m}, z_{i-1,m}, \Delta s, \Delta t) = 0 \tag{6}$$

Since z at the $m-1$, $m-2$, and $m-3$ time stations is known at m from preceding calculations or is determined from initial conditions, Eq. (6) may be treated as being essentially independent of time. Equation (6) together with three boundary conditions at the pole point and three at the edge of the shell define the problem to be solved and must be solved simultaneously to determine z at the mth time step. Because they are nonlinear, the equations are linearized using an iterative Newton-Raphson procedure (Ref. 18). For convenience in the solution of the simultaneous equations, the vector z_i is partitioned into two three-element ordered subvectors x_i and y_i.

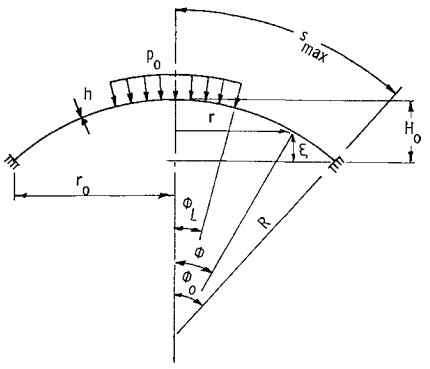

Fig. 1 Shell geometry and loading.

Use of a Taylor's expansion for Eqs. (2) and (6) yields

$$(\delta F_j/\delta x_1)\delta x_1 + (\delta F_j/\delta y_1)\delta y_1 = -F_j(\bar{x}_1,\bar{y}_1,s) \tag{7}$$

$$(\delta f_k/\delta x_{i-1})\delta x_{i-1} + (\delta f_k/\delta y_{i-1})\delta y_{i-1} + (\delta f_k/\delta x_i)\delta x_i + (\delta f_k/\delta y_i)\delta y_i = -f(\bar{x}_i,\bar{y}_i,\bar{x}_{i-1},\bar{y}_{i-1},\Delta s) \qquad i = 2, 3, \ldots n \tag{8}$$

$$(\delta G_j/\delta x_n)\delta x_n + (\delta G_j/\delta y_n)\delta y_n = -G_j(\bar{x}_n,\bar{y}_n,s) \tag{9}$$

where $j = 1, 2, 3$ and $k = 1, 2 \ldots 6$ and n is the total number of spatial stations. F_j is a functional representation of Eq. (2) at the boundary $i = 1$ and G_j is a functional representation of Eq. (2) at the edge, $i = n$. Also

$$\delta x_i = x_i - \bar{x}_i, \quad \delta y_i = y_i - \bar{y}_i \tag{10}$$

and $\{x_i,y_i\}$ is the solution vector and $\{\bar{x}_i,\bar{y}_i\}$ is the approximate solution vector to Eqs. (2) and (6). The iterative procedure is established whereby

$$\bar{x}_i^{r+1} = \bar{x}_i^r + \delta x_i$$
$$\bar{y}_i^{r+1} = \bar{y}_i^r + \delta y_i \tag{11}$$

and the superscript, r, indicates the rth iteration cycle. When $\{\delta x_i,\delta y_i\}$ vanish convergence has been obtained. The set of equations (7–9) take the form of a five-diagonal-banded matrix where each element is a 3×3 matrix. The set of equations (7–9) is solved by using a modified Potters' method (Ref. 15 or 19) for banded matrices. This analysis and numerical solution has been programed in FORTRAN IV for use on a CDC 6600 computer and the resulting computer program provides the capability for nonlinear static and dynamic analysis of a general orthotropic shell of revolution subjected to axisymmetric thermal or mechanical loads and having arbitrary boundary conditions at each end of the shell.

The physical geometry of the isotropic spherical cap and the loading considered with the program in the present study are shown in Fig. 1. The positive directions on the elements of z, force and moment resultants, and surface pressures are shown in Fig. 2. Results for three separate boundary conditions at the shell edge ($i = n$) are obtained. They are defined as follows:

1) clamped

$$u_n = w_n = \beta_n = 0 \tag{12}$$

2) simply supported

$$u_n = w_n = m_{11,n} = 0 \tag{13}$$

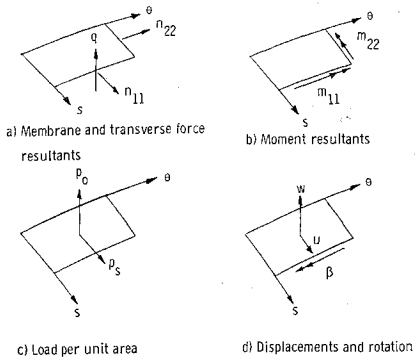

Fig. 2 Positive sense of forces, moments, loads, displacements, and rotation.

3) unrestrained

$$n_{11,n}\cos\varphi_0 + q_n\sin\varphi_0 = 0$$
$$u_n\sin\varphi_0 - w_n\cos\varphi_0 = 0, \quad m_{11,n} = 0 \tag{14}$$

where φ_0 is maximum shell angle defined in Fig. 1. The unrestrained edge differs from the simple support in that radial motion is freely allowed. The pole conditions at $i = 1$ are

$$q_1 = \beta_1 = u_1 = 0 \tag{15}$$

The results in this report are also based on 26 meridional stations, a Poisson's ratio of 0.3, and a $\Delta\tau$ of 0.10. All dynamic loads are step pulses of infinite duration ($\tau^* = \infty$) and the initial conditions are that the initial displacements (u,w) and velocities ($\dot{u},\dot{w}$) of the shell vanish. This implies

$$z_{i,0} = \dot{z}_{i,0} = 0 \tag{16}$$

Both the static and dynamic loads are uniformly distributed axisymmetric pressure loads of magnitude p_0 that cover a given percentage of the center surface area of the shell (Fig. 1).

Buckling Criteria

Static Top-of-the-Knee Buckling

Suitable criteria for determining static "top-of-the-knee" axisymmetric buckling loads are well known (see, for example, Ref. 3) and problems only arise in the numerical determination of such buckling loads. The procedure used in the present study to determine static buckling loads is to increment the load until the Newton-Raphson method fails to converge for a load level. The load increment is then reduced to one-fifth the previous load increment and load incrementation is again initiated from the last converged load level. Whenever convergence again fails, this procedure of reducing the load increment by a factor of five is repeated. When convergence fails

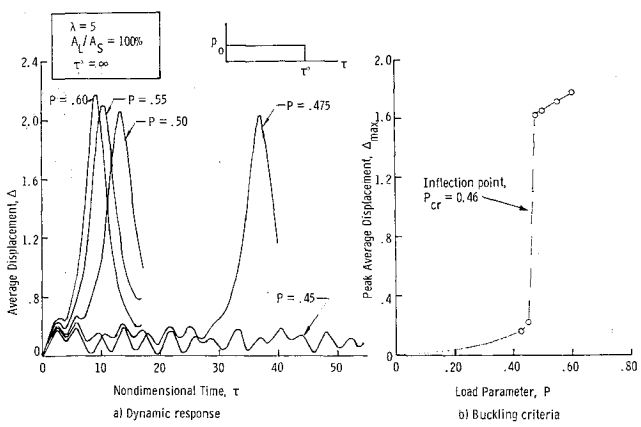

Fig. 3 Dynamic buckling load for a clamped spherical cap.

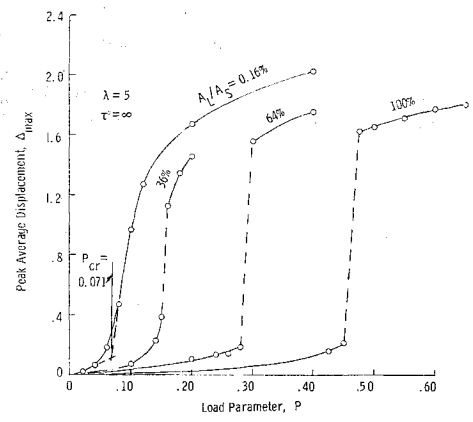

Fig. 4 Peak average displacement curves of various centrally distributed dynamic loads on clamped spherical caps.

on the fourth reduction of load increment, the last converged load level is taken as the buckling load. The initial increment was taken to be approximately one-fifth of the resulting buckling load.

To insure that a maximum point has been reached in the load vs deformation curve, a top-of-the-knee check is made by incrementing the deformation state sufficiently to cross over the top of the knee. This is accomplished by taking the difference in the last two converged deformation states times some arbitrary factor (normally 5) and adding it to the last converged (prebuckled) deformation state. Beginning with this state, the equations are iterated until an equilibrium state is found in this neighborhood. The load is then reduced one load increment to move down the opposite side of the knee and confirm that a maximum was reached.

Dynamic Buckling

The criteria used to determine buckling under dynamic loads are not as well defined as for static loads and require an evaluation of the transient response of the shell for various load levels. The criteria in most common use (for example, Refs. 5 and 8) are based on plots of the peak nondimensional average displacement, Δ_{max}, of the structure vs the amplitude of the load where Δ is the average displacement nondimensionalized with respect to the average height of the undeformed shell. Thus

$$\Delta = \int_0^{r_0} rwdr \Big/ \int_0^{r_0} r\xi dr \tag{17}$$

where ξ, r, and r_0 are defined in Fig. 1.

There is a load range where a sharp jump in peak average displacement occurs for a small change in load amplitude.

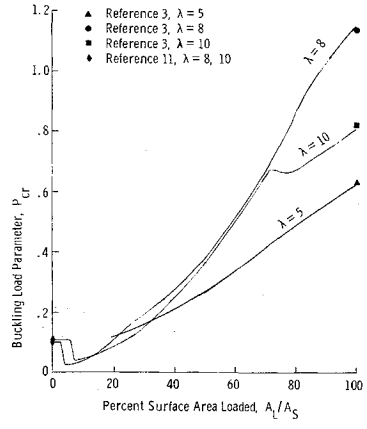

Fig. 5 Axisymmetric buckling load parameter vs percent surface area loaded for clamped spherical caps.

The inflection point of the load deflection curve in this range is taken as the buckling load and the method is denoted the "inflection point method" in Ref. 8. The method is illustrated by the typical example shown in Fig. 3. Time histories of Δ are shown in Fig. 3a for a clamped spherical cap of shell parameter $\lambda = 5$ for several values of uniformly distributed load parameter P. Here P is

$$P = p_0 A_L / p_{CL} A_S \tag{18}$$

where p_0 is the magnitude of the compressive lateral pressure, p_{CL} is the classical buckling pressure for a closed spherical shell

$$p_{CL} = \{2E/[3(1 - \nu^2)]^{1/2}\}(h/R)^2 \tag{19}$$

R and h are the shell radius and thickness, E is Young's modulus, and ν is Poisson's ratio. The quantity A_L is the surface area on which p_0 acts and is given by

$$A_L = 2\pi R^2\{1 - \cos\varphi_L\} \tag{20}$$

and A_S is the total surface area of the shell

$$A_S = 2\pi R^2\{1 - \cos\varphi_0\} \tag{21}$$

where φ_L is the angle between the shell axis and the normal to the shell at edge of the loaded region as defined in Fig. 1.

If the peak average displacements for the cap from Fig. 3a are plotted vs load amplitude, the curve given in Figure 3b results. It is clear from the rapid change in deflection behavior in the plot that a buckling load range has been defined. Since the inflection point on such a plot is difficult to pinpoint, it is usually estimated as the average of the two load values which bracket the rapid change in deflection behavior. Thus, the axisymmetric buckling load P_{cr} is approximately 0.46. Obviously, for values of shell and load parameters corresponding to such abrupt behavior, an estimate of the inflection point serves as a suitable reference value for the buckling load.

Consider, however, the response characteristics of the shell subjected to a load centrally distributed over less than the total surface area. Figure 4 shows plots of peak average displacement vs load for several percentages of the ratio A_L/A_S. The curve for a 0.16% loaded area (i.e., a highly concentrated pressure) shows that the inflection point criterion may not be a suitable criterion for buckling. Even in cases where the change in the Δ_{max} vs P curve is more dramatic (such as for the 36, 64, and 100% loadings) it would appear that a more conservative criterion might well be used such as a point at which Δ begins to change rapidly near the knee in the curve below the inflection point. This point must, of course, be somewhat arbitrary but such a choice appears reasonable from an engineering point of view. The threshold load is taken as some load beyond which small changes in load lead to large increases in displacement. An example, which defines the threshold as the intersection point of two tangents, is shown graphically for the 0.16% curve in Fig. 4 yielding $p_{cr} = 0.071$. This procedure was selected in the present study for defining

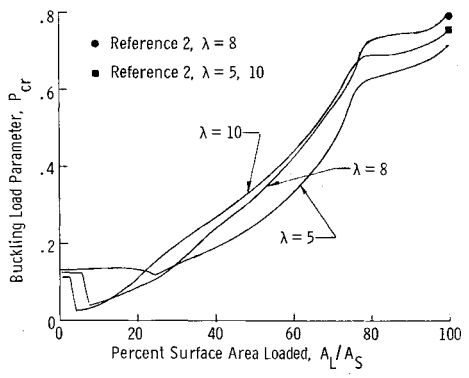

Fig. 6 Axisymmetric buckling load parameter vs percent surface area loaded for simply supported spherical caps.

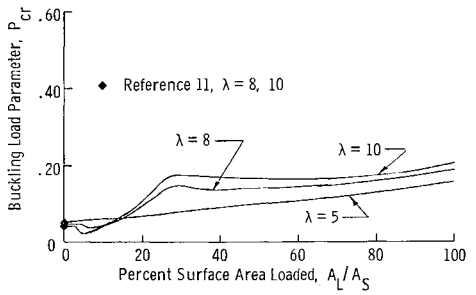

Fig. 7 Axisymmetric buckling load parameter vs percent surface area loaded for unrestrained spherical caps.

dynamic buckling loads. It has the advantage that when the change is dramatic, the results essentially agree with those obtained by the inflection point method, and it provides a meaningful but more conservative criterion for handling highly localized loads.

Results and Discussion

Static Buckling Results

Consider, first, buckling under centrally distributed static loads. Figures 5, 6, and 7 present the results for axisymmetric buckling loads for the cases of clamped, simply supported, and unrestrained edges, respectively, as a function of surface area loaded. In Fig. 5, the results for a fully loaded clamped shell (i.e., $A_L/A_S = 100\%$) agree with those given in Ref. 3. As the load becomes concentrated at the center of the shell (i.e., $A_L/A_S \rightarrow 0$), the results approach those for a concentrated load given in Ref. 11. For the case of $\lambda = 5$, the shell does not buckle axisymmetrically when loaded over less than 20% of the area; this is reasonable since it has been shown in Ref. 10 that top-of-the-knee buckling does not occur for concentrated loads where $\lambda \leq 7$. The results of Fig. 6 for 100% loading agree with those of Ref. 2 for a uniformly loaded shell as noted on the figure, and the results of Fig. 7 for a nearly 0% loading correspondingly agree with those of Ref. 11 for a concentrated load.

Figures 5, 6, and 7 describe the shell buckling load behavior during the load transition from a uniform load to a highly concentrated load. An understanding of this behavior is best accomplished by studying a representative curve in detail. This is done in Fig. 8a where the curve for a simply supported cap with $\lambda = 8$ given on Fig. 6 has been replotted. Also shown

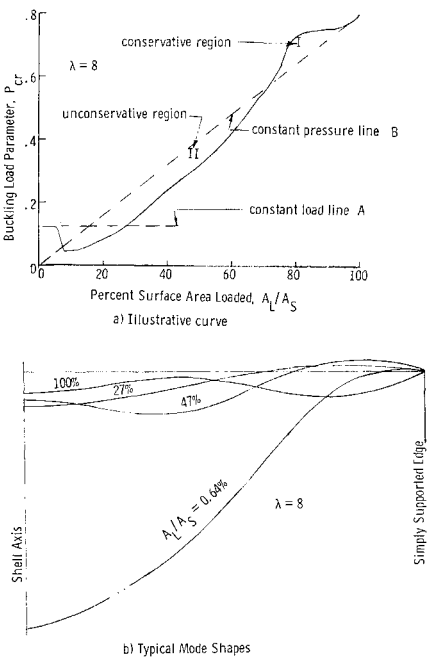

Fig. 8 Corresponding mode shapes and axisymmetric buckling loads for simply supported spherical caps.

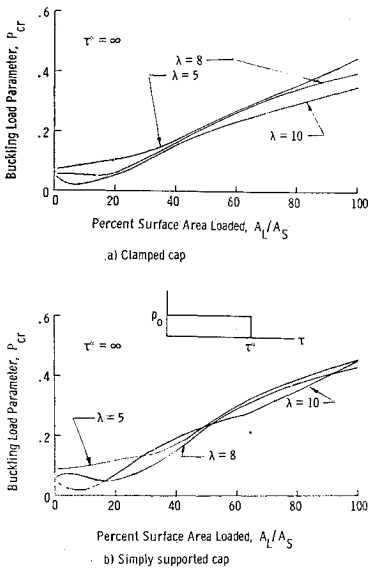

Fig. 9 Axisymmetric dynamic buckling loads for various λ and centrally distributed loads.

on Fig. 8a as dotted lines are two limiting cases. Line A corresponds to the assumption of a constant buckling load magnitude equal to that of a concentrated load. Line B corresponds to the assumption of constant pressure equal to that of the fully loaded uniform pressure. The $\lambda = 8$ curve has several characteristics. Near the 0% loaded area when the load is nearly a concentrated load, the assumption of a concentrated load adequately predicts the buckling load. At approximately 5% loaded area there is a sharp drop in buckling load magnitude to below even the constant pressure line. As the loaded area is increased, the buckling load increases; however, the pressure is less than that of a uniformly loaded shell. When the load is distributed over more than 72% of the shell surface, the buckling pressure exceeds and finally becomes equal to the fully loaded buckling pressure. The sharp drop in buckling load for a 5% loaded area is interesting because it indicates that neither the assumption of a concentrated load nor a uniform pressure is a conservative estimate of buckling load. An understanding of this behavior can be obtained by noting that results similar to these were observed experimentally in Ref. 12 where it was shown that, as the radius of the loading surface was increased, local and somewhat benigned buckling occurred at lower load magnitude.

The other characteristics of the curve are due to the change in buckling mode shapes resulting from changes in loaded area. Figure 8b shows an ensemble of buckling mode shapes for several typical loaded areas ranging from a nearly concentrated load of $A_L/A_S = 0.64\%$ to the fully loaded case. Figure 8b shows the dramatic changes in buckling shape which result as the load is distributed over different areas and shows why one should not expect either the concentrated load or uniform pressure assumptions to be representative of all ranges of the loaded area parameter.

The characteristics of the curve in Fig. 8a are generally typical of all the curves contained in Figs. 5–7 although there are differences for all curves. For the very low values of A_L/A_S less than 3–5%, the assumption of a concentrated load is reasonable for obtaining buckling loads. For high values of A_L/A_S greater than 75–95%, assumption of a uniformly distributed pressure is reasonable. In between these two extremes, the assumption of a constant uniform pressure is a crude approximation to the axisymmetric buckling load. This assumption cannot be relied on, however, to give conservative estimates of axisymmetric buckling load and may, in some cases, be in error by a factor of 2 on the unconservative side. On Fig. 8a for example, this assumption would be conservative for region I and unconservative for region II.

The influence of moment boundary condition on buckling loads can be seen by comparing the results of Fig. 5 with those of Fig. 6. This comparison shows that when buckling is restricted to be axisymmetric, clamping can raise the buckling load (e.g., for $\lambda = 8$ and 100% loading P_{cr} increases from 0.794 for a simply supported edge to 1.145 for a clamped edge) and can lower the buckling loading load (e.g., for $\lambda = 5$ and 100% loading P_{cr} decreases from 0.713 for a simply supported edge to 0.622 for a clamped edge). This behavior is also the result of changes in the buckling mode shape caused by changes in boundary conditions.

The influence of lateral restraint on the buckling load can be seen by comparing the results in Figs. 6 and 7. This comparison shows that removing the lateral restraint at the boundary generally leads to sharp reductions in buckling loads by factors of 2 to 4. There are, however, limited parameter ranges such as, for example, the $\lambda = 8$, $A_L/A_S = 20\%$ case where removing the inplane restraint leads to equal or slightly larger buckling loads.

Dynamic Buckling Results

Figure 9a gives the total load for the axisymmetric buckling of a clamped shallow cap with $\lambda = 5$, 8, and 10 subjected to infinite duration axisymmetric step loads ($\tau^* = \infty$) distributed over various percentages of the cap area. Figure 9b gives similar results for the case of a simply supported cap. In general, the plots for dynamic buckling are smoother than the static buckling curves, but have the same characteristics with the exception that the dynamic buckling loads are lower than static buckling loads. In addition, because of the dynamic buckling criteria used, all shell parameters exhibit a dynamic buckling load including the clamped $\lambda = 5$ case near the origin. Such dynamic buckling loads appear to be reasonably safe loads that can be applied to the structure without undue deflections taking place.

Although the dynamic response curves are not shown for most cases, it was necessary to investigate the dynamic response over fairly long periods of time to insure that the structure did not eventually buckle. This becomes more important for the larger shell parameters such as $\lambda = 8$ and $\lambda =$

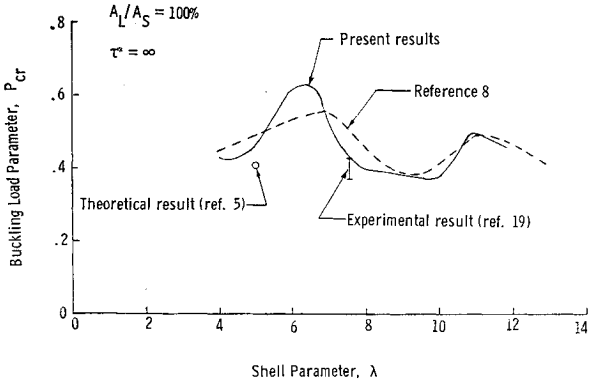

Fig. 10 Comparisons of axisymmetric dynamic buckling loads of various λ for clamped spherical caps.

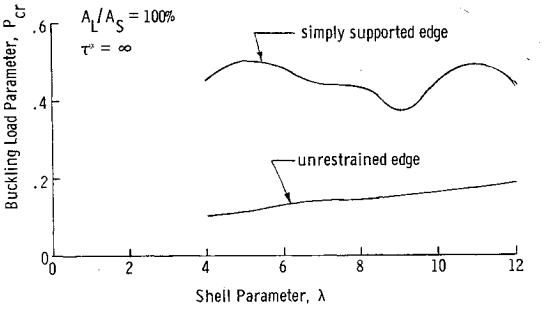

Fig. 11 Comparison of axisymmetric dynamic buckling loads for simply supported and unrestrained edges.

10. For some load levels at higher λ's the response was studied out to $\tau = 120$. The necessity for carrying the response calculations out over a long period of time is demonstrated by noting that Ref. 8 considered the clamped spherical cap whose response curves are shown in Fig. 3 and concluded that the axisymmetric buckling load was 0.49 based on reported response times up to $\tau = 14$. The present calculations show that if the response is carried to $\tau = 60$, the buckling load is reduced to 0.46. Note that for a shallow spherical cap made of aluminum and having a radius-thickness ratio of 100, a nondimensional time of 100 is an actual time of 0.0050 sec. Although damping would affect the results in a real structure, it is questionable whether short-time buckling calculations covering only the first few response cycles are sufficient to determine safe buckling loads. Furthermore, late response buckling results were found experimentally in Ref. 20 where spherical caps with $\lambda = 7.5$ exhibited 9 cycles of vibration prior to buckling. Since there are no adequate criteria for defining dynamic buckling which include the effect of the response duration, the procedure used in this study was to trace the maximum subcritical response 10 nondimensional time units past the point where the last supercritical buckling occurred to see if any growth in deflection could be observed.

The ratio of dynamic to static axisymmetric buckling loads can be obtained by comparing Figs. 9a and 9b with Figs. 5 and 6, respectively. In general, the dynamic buckling loads are less than static buckling loads for most of the parameter ranges; however, no simple ratio holds for all shell parameters and loaded area. It is also seen that the variation of dynamic buckling load with loaded area is smoother than in the static case, but there is still a decrease in buckling load resulting from spreading a central concentrated load over a small but finite area.

Figure 10 gives a plot of dynamic buckling load of a fully loaded clamped shell as a function of shell parameter. The present results agree fairly well with those in Ref. 8 and were expected to be slightly lower because the present results consider longer response times and a more conservative buckling criteria. This is basically true except for the $\lambda = 6$ region where the present results exceed those of Ref. 8. Numerical results for $\lambda = 6$ were not included in Ref. 8 and an increase in buckling strength in this parameter range appears to have been missed. The present results agree fairly well at $\lambda = 5$ with five-degree-of-freedom results of Ref. 5. Particularly encouraging is the close agreement at $\lambda = 7.5$ with experimental results of Ref. 20. Figure 11 shows similar buckling load plots vs λ for fully loaded shells with simply supported restrained and unrestrained boundaries. Figure 12 shows results for the variation of buckling load vs area loaded for a cap with $\lambda = 8$ and for the three boundary conditions of clamped, simply supported, and unrestrained. Comparison of the results in Figs. 11 and 12 shows that the introduction of horizontal edge restraint substantially increases the buckling load for an essentially fully loaded shell and for a highly concentrated load. Comparison of the clamped and simply supported restrained curves in Fig. 12 shows that rotational restraint has less effect on buckling load than does horizontal restraint. The results in Fig. 12 also show a loaded area region between approximately 20%–35% where the buckling load is essentially independent of boundary conditions.

Concluding Remarks

An investigation of static and dynamic axisymmetric buckling of shallow spherical caps subjected to centrally distributed symmetric loads has been carried out. The results are based on a numerical solution to Sanders' nonlinear shell equations subjected to either static or dynamic loads. Buckling loads have been obtained for clamped, simply supported, and unrestrained edges of spherical caps subjected to a constant static pressure or a step pulse of infinite duration distributed axisymmetrically over a center portion of the shell. The results show that for a shell almost fully loaded, the buckling pressure is essentially that of a fully loaded shell, and for the case where the load is distributed approximately over 3–5% or less of the shell surface, the load can be considered concentrated. Between these two extremes, however, neither the assumption of a concentrated load nor uniform pressure can be relied on to give a conservative estimate of the buckling load. Results for dynamic buckling loads were generally less than static buckling loads; however, no simple ratio exists between static and dynamic buckling loads, which holds for all load conditions and/or shell parameters. Comparisons of buckling load vs loaded area show that spreading a concentrated static load over a small but finite area can lower the buckling load substantially. Although changes are not so dramatic, the same phenomenon occurs for dynamic step loads. Results for simply supported and clamped edges show that when buckling is axisymmetric clamping edges may either increase or decrease the buckling load of the shell for both static and dynamic buckling, depending on the load condition and shell geometry. Results also show that removing the lateral boundary restraints can substantially decrease static and dynamic buckling loads.

The results of this study are restricted to axisymmetric buckling, and the inclusion of asymmetric behavior is necessary to completely define buckling loads over the full parameter range. The results show that the buckling behavior of a partially loaded shell is quite complex and buckling loads cannot be inferred from results for the extreme cases of uniform and concentrated loading.

Appendix: Definition of Matrix Elements

The vector z of unknowns contained in Eq. (1) at a point i is divided into two subvectors x_i and y_i; where x_i and y_i are the force and displacement vectors

$$x_i = \begin{Bmatrix} n_{11} \\ q \\ m_{11} \end{Bmatrix}_i; \quad y_i = \begin{Bmatrix} u \\ w \\ \beta \end{Bmatrix}_i \tag{A1}$$

Positive direction of quantities are shown in Fig. 2. The nonzero elements of the H matrix are

$$\left.\begin{aligned}
&h_{11}/(1 - G_6) = h_{22} = -h_{31}/G_2 = h_{44}/G_6 = \\
&\qquad h_{33}/(1 - G_3) = -\rho^{-2}h_{46}/G_2 = h_{66}/G_3 = \cos\varphi/r \\
&h_{12} = -h_{21} - G_6\frac{\sin\varphi}{r} = h_{45} - G_6\frac{\sin\varphi}{r} = \\
&\qquad -h_{54} = \varphi' \\
&\frac{h_{13}}{\cos\varphi} = \frac{h_{23}}{\sin\varphi} = \frac{\rho^2 h_{64}}{\cos\varphi} = \frac{\rho^2 h_{65}}{\sin\varphi} = -\frac{G_7}{r} \\
&h_{14}/\cos^2\varphi = h_{15}/\cos\varphi\sin\varphi = h_{24}/\cos\varphi\sin\varphi = \\
&\qquad h_{25}/\sin^2\varphi = -(G_8 + C_{22})/r^2 \\
&\frac{h_{16}}{\cos\varphi} = \frac{h_{26}}{\sin\varphi} = \frac{(G_1 + K_{22})\cos\varphi}{r^2}\rho^2; h_{32} = h_{56} = -1 \\
&\frac{h_{34}}{\cos\varphi} = \frac{h_{35}}{\sin\varphi} = -\frac{(G_4 + \rho^{-2}K_{22})\cos\varphi}{r^2} \\
&h_{36} = \frac{(G_5 + \rho^{-2}D_{22})\cos^2\varphi}{r^2} \\
&\frac{\rho^2 h_{41}}{D_{11}} = \frac{h_{43}}{K_{11}} = -\frac{\rho^2 h_{61}}{K_{11}} = \frac{h_{63}}{C_{11}} = \frac{1}{G}
\end{aligned}\right\} \tag{A2}$$

The nonzero elements of the 6×6 $\tilde{H}$ matrix are

$$\left.\begin{aligned}
&\tilde{h}_{11} = \varphi'\beta/\eta; \tilde{h}_{21} = \beta\cos\varphi/r\eta + \beta'/\eta \\
&\tilde{h}_{26} = n'_{11}/\eta; \tilde{h}_{46} = \beta/2\eta
\end{aligned}\right\} \tag{A3}$$

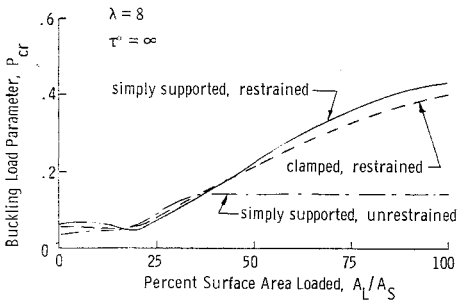

Fig. 12 Axisymmetric dynamic buckling loads for various boundary conditions and centrally distributed loads.

The nonzero elements of the six element e vector are

$$\left.\begin{aligned} e_1 &= -p_s + \frac{\cos\varphi}{r}\{G_6 t_1^n + G_7 t_1^m - t_2^n\} \\ e_2 &= -p_0 + \frac{\sin\varphi}{r}\{G_6 t_1^n + G_7 t_1^m - t_2^n\} \\ e_3 &= (\cos\varphi/r)\{G_2 t_1^n + G_3 t_1^m - t_2^m\} \\ e_4 &= (D_{11}/\rho^2 G)t_1^n - (K_{11}/G)t_1^m \\ e_6 &= (t_1^n/\rho^2 G)K_{11} - (t_1^m/G)C_{11} \end{aligned}\right\} \quad \text{(A4)}$$

The nonzero elements of the 6×6 f matrix are

$$f_{14} = f_{25} = 1 \quad \text{(A5)}$$

The constant terms in Eqs. (A2–A5) are

$$\left.\begin{aligned} &G = -\rho^2(C_{11}D_{11} - K_{11}^2), \quad G_1 = -\rho^{-2}G_2C_{12} - K_{12}G_3 \\ &G_2 = \rho^{-4}(D_{11}K_{12} - D_{12}K_{11})/G, \quad G_3 = \rho^{-2}(C_{11}D_{12} - K_{11}K_{12})/G \\ &G_4 = \rho^{-2}G_1, \quad G_5 = -K_{12}G_2 - \rho^{-2}D_{12}G_3 \\ &G_6 = \rho^{-2}(C_{12}D_{11} - K_{11}K_{12})/G, \quad G_7 = (C_{11}K_{12} - C_{12}K_{11})/G \\ &G_8 = -C_{12}G_6 - \rho^{-2}K_{12}G_7 \end{aligned}\right\} \quad \text{(A6)}$$

The terms φ and r are defined in Fig. 1 and the C_{ij}, K_{ij}, and D_{ij} constants arise from the general nondimensional orthotropic constitutive relationships

$$\begin{Bmatrix} n_{11} \\ n_{22} \\ m_{11} \\ m_{11} \end{Bmatrix} = \begin{bmatrix} C_{11} & C_{12} & K_{11} & K_{12} \\ C_{12} & C_{22} & K_{12} & K_{22} \\ \rho^{-2}K_{11} & \rho^{-2}K_{12} & D_{11} & D_{12} \\ \rho^{-2}K_{12} & \rho^{-2}K_{22} & D_{12} & D_{22} \end{bmatrix} \begin{Bmatrix} e_{11} \\ e_{22} \\ \kappa_{11} \\ \kappa_{22} \end{Bmatrix} - \begin{Bmatrix} t_1^n \\ t_2^n \\ t_1^m \\ t_2^m \end{Bmatrix} \quad \text{(A7)}$$

Here n_{11} and m_{11} are the force resultants defined in Fig. 2 and e_{11} and κ_{11} are the tensor strains and curvatures. The terms t_1^n and t_1^m are the induced thermal forces and moments.

In Eqs. (A7) the nondimensional C_{ij}, D_{ij}, and K_{ij} terms for the isotropic material used in this presentation are

$$\left.\begin{aligned} &C_{11} = C_{22} = 1/(1-\nu^2), \; C_{12} = \nu C_{11} \\ &D_{11} = D_{22} = C_{11}/12, \; D_{12} = \nu D_{11} \\ &K_{11} = K_{12} = K_{22} = 0 \end{aligned}\right\} \quad \text{(A8)}$$

and the induced isotropic temperature resultants are

$$\left.\begin{aligned} t_i^n &= [\bar{\alpha}\eta/(1-\nu)]\int T(\zeta)d\zeta \\ t_i^m &= [\bar{\alpha}\eta/(1-\nu)]\int T(\zeta)\zeta d\zeta \end{aligned}\right\} \quad \text{(A9)}$$

where the subscript i refers to the principal directions, $\bar{\alpha}$ is the thermal coefficient of expansion, ζ is the normal distance from the middle surface and $T(\zeta)$ is the expression for the temperature change along the shell cross section.

References

[1] Huang, N. C., "Unsymmetrical Buckling of Thin Shallow Spherical Shells," *Transactions of the ASME, Series E, Journal of Applied Mechanics*, Sept. 1964, pp. 447–457.

[2] Weinitschke, H. J., "On Asymmetric Buckling of Shallow Spherical Shells," *Journal of Mathematics and Physics*, March 1965, pp. 141–163.

[3] Budiansky, B., "Buckling of Clamped Shallow Spherical Shells," *Proceedings of the Symposium on the Theory of Thin Elastic Shells, Delft*, North Holland, Amsterdam, Holland, 1959, p. 64.

[4] Evensen, D. A. and Fulton, R. E., "Some Studies on the Nonlinear Dynamic Response of Shell-Type Structures," *Dynamic Stability of Structures*, edited by G. Herrman, Pergamon Press, New York, 1967, pp. 237–254.

[5] Budiansky, B. and Roth, R. S., "Axisymmetric Dynamic Buckling of Clamped Shallow Spherical Shells," TN D-1510, 1962, NASA, pp. 597–606.

[6] Koga, T. and Hoff, N. J., "The Axisymmetrical Buckling of Initially Imperfect Complete Spherical Shells," SUDAAR 332, May 1968, Stanford Univ.

[7] Humphrey, J. S. and Bodner, S. R., "Dynamic Buckling of Shallow Shells Under Impulsive Loading," *Journal of the Engineering Mechanics Division, Proceedings of the American Society of Civil Engineers*, ASCE 88, No. EM2, 1962, pp. 17–36.

[8] Huang, N. C., "Axisymmetric Dynamic Snap-Through of Elastic Clamped Shallow Spherical Shells," AFOSR-68-0469, TR-7, Feb. 1968, Air Force Office of Scientific Research.

[9] Fitch, J. R., "The Buckling and Post-Buckling Behavior of Spherical Caps Under Concentrated Loads," *International Journal of Solids and Structures*, Vol. 4, 1968, pp. 421–446.

[10] Mescall, J. F., "On the Numerical Analysis of the Nonlinear Axisymmetric Equations for Shells of Revolution," AMRA TR 64-20, Oct. 1964.

[11] Mescall, J. F., "Large Deflection of Spherical Shells Under Concentrated Loads," *Transactions of the ASME*, Brief Note, Dec. 1965, pp. 936–938.

[12] Penning, F. A. and Thurston, G. A., "Buckling of Elastic Shells Under Concentrated Load," Martin CR-65-11, Contract NASw-912, April 1965, NASA.

[13] Fulton, R. E. and Barton, F. W., "Dynamic Buckling of Shallow Arches," presented at ASCE EMD Specialty Conference, Raleigh, N.C., Nov. 1967, pp. 49–52.

[14] Sanders, J. L., Jr., "Nonlinear Theories for Thin Shells," *Quarterly of Applied Mathematics*, Vol. XXI, 1963, pp. 21–36.

[15] Budiansky, B. and Radkowski, P. P., "Numerical Analysis of Unsymmetrical Bending of Shells of Revolution," *AIAA Journal*, Vol. 1, No. 8, Aug. 1963, pp. 1833–1842.

[16] Houbolt, J. C., "A Recurrence Matrix Solution for the Dynamic Response of Aircraft in Gusts," Rept. 1010, 1951, NACA.

[17] Johnson, D. E. and Grief, R., "Dynamic Response of Cylindrical Shell. Two Numerical Methods," *AIAA Journal*, Vol. 4, No. 3, March 1966, pp. 486–494.

[18] Sylvester, R. J. and Meyer, F., "Two Point Boundary Problems by Quasilinearization," *SIAM Journal*, Vol. 13, No. 2, June 1965, pp. 586–602.

[19] Potters, J. L., "A Matrix Method for the Solution of a Second Order Difference Equation in Two Variables," Rept. MR 19, 1955, Mathematics Centrum, Amsterdam, Holland.

[20] Lock, M. H., Okubo, S., and Whittier, J. S., "Experiments on the Snapping of a Shallow Dome Under a Step Pressure Load," Air Force Rept. SSD-TR-67-117; also Aerospace Rept. TR-1001(2240-30)-8, June 1967, Aerospace Corp., El Segundo, Calif.